

Article

Applying International Power Quality Standards for Current Harmonic Distortion to Wave Energy Converters and Verified Device Emulators

James Kelly ^{1,*} , Endika Aldaiturriaga ² and Pablo Ruiz-Minguela ³

¹ MaREI Centre, Environmental Research Institute, University College Cork, Ringaskiddy P43 C573, Ireland

² IDOM Consulting, Engineering, Architecture, 48015 Bilbao, Spain; ealdaiturriaga@idom.com

³ Tecnalia, Parque Científico y Tecnológico de Bizkaia Astondo Bidea, Edificio 700, E-48160 Bizkaia, Spain; jpablo.ruiz-minguela@tecnalia.com

* Correspondence: james.kelly@ucc.ie

Received: 20 June 2019; Accepted: 20 September 2019; Published: 24 September 2019



Abstract: The push for carbon-free energy sources has helped encourage the development of the ocean renewable energy sector. As ocean renewable energy approaches commercial maturity, the industry must be able to prove it can provide clean electrical power of good quality for consumers. As part of the EU funded Open Sea Operating Experience to Reduce Wave Energy Cost (OPERA) project that is tasked with developing the wave energy sector, the International Electrotechnical Commission (IEC) developed electrical power quality standards for marine energy converters, which were applied to an oscillating water column (OWC). This was done both in the laboratory and in the real world. Precise electrical monitoring equipment was installed in the Mutriku Wave Power Plant in Spain and to an OWC emulator in the Lir National Ocean Test Facility at University College Cork in Ireland to monitor the electrical power of both. The electrical power generated was analysed for harmonic current distortion and the results were compared. The observations from sea trials and laboratory trials demonstrate that laboratory emulators can be used in early stage development to identify the harmonic characteristics of a wave energy converter.

Keywords: renewable energy; ocean energy; wave energy; oscillating water column; power quality; current harmonic distortion; IEC standards; modelling

1. Introduction

The Paris Climate Agreement highlighted the global consensus that a low carbon energy strategy needs to be established. The development of clean renewable energy represents a piece of the greater low carbon energy mix, and it has been a growing part of the energy sector this millennium. Wind, solar, and hydropower plants accounted for 90% of the installed renewable generation capacity in the European Union in 2017 [1]. The ocean energy sector, which includes wave and tidal energy, has shown promise for further diversifying the European renewable energy portfolio, but the sector remains in the maturation process and has yet to prove commercial viability. One subsection of the ocean energy sector, wave energy, has been making progress towards commercialisation in recent years [2,3]. This progress includes several large-scale, bottom-fixed shoreline oscillating water columns (OWC), which have been successfully grid-connected [4–6].

A boost to the maturation of the ocean renewable energy field has been the development of the International Electrotechnical Commission (IEC) 62600 standardisation for marine energy converters (MEC), which includes wave, tidal, and other current converters. The European Union Horizon 2020 funded Open Sea Operating Experience to Reduce Wave Energy Cost (OPERA) project is a four-year project with multiple objectives designed to help further the growth of the ocean renewable

energy sector and bring it closer to commercialisation. One of the objectives of the OPERA project is to apply some of the recently developed IEC 62600 standards to an OWC wave energy converter (WEC). The standards applied in the OPERA project include the IEC 62600-30: Electrical power quality requirements for wave, tidal, and other water current energy converters.

As part of the maturation process, the ocean renewable energy sector must prove that it can provide consistent electricity with power quality at a level that is safe and non-disruptive to both private and commercial consumers [7]. Power quality concerns of ocean renewable energy converters have been known for years and models have been built to help identify problems that can arise from grid-connected converters [8,9]. Methods have also been developed and tested to mitigate power quality issues caused by WECs [10]. However, internationally accepted standards for the power quality of WECs have not been tested to date, nor are there many instances where models for renewable energy converters of any time used for power quality assessment are verified against real-world data. The OPERA project offers a unique opportunity to apply IEC power quality standards to sea trials from a grid-connected and fully operational WEC and use the data collected from the sea trials to verify laboratory generated data from a model working with a hardware-in-the-loop (HIL) WEC emulator.

The sea trial data were generated by the Mutriku Wave Power Plant (MWPP), which played an intricate role during the OPERA project, as it was utilised for experimentation and data collection [11,12]. The MWPP is a 175 kW OWC array built into the breakwater in Mutriku, Spain, on the Bay of Biscay [5]. For the application of the IEC 62600-30 standards, the MWPP electrical power take-off (PTO) system was retrofitted with a Supervisory Control and Data Acquisition (SCADA) system to the requirements of the specifications. The SCADA was active for a period of four months, where it collected two datasets per day for further analysis, and those datasets were used to determine harmonic current distortion caused by the OWC array. The laboratory trials were performed at the Lir National Ocean Test Facility (NOTF) within the MaREI Centre at University College Cork (UCC), Ireland using a 25 kW HIL-based WEC emulator [13,14]. The data collection and analysis methods for both the sea trial and laboratory trial testing are presented in this paper, along with the results of the harmonic current distortion analysis.

2. Data Collection and Analysis Methods

The international technical specification IEC 62600-30 focuses on power quality issues and parameters for single-phase and three-phase, grid-connected and off-grid MECs. Poor electrical power quality negatively affects both power sources and loads, so this technical specification was produced to establish measurement methods, application techniques, and results interpretation guidelines to account for the electrical performance of MECs.

The measurement procedures specified in the IEC 62600-30 are valid for a single MEC unit with a three-phase grid or an off-grid connection. They are designed to be as non-site-specific as possible. For analytical purposes, the IEC 62600-30 divides marine renewable energy resources into three classifications: low, medium, and high. For WECs, the resources can be classified through the sea summary statistics using either significant wave height (H_s) or energy period (T_e). The decision of which statistic to use is made by the developer, as is the parsing of the resource classification, though the classifications should be based annual conditions of the deployment site. The procedures are valid for any size of MEC, with varying specifications depending on the type of voltage connection, which includes three classes of connection, low voltage (LV), medium voltage (MV), and high voltage (HV).

In this paper, the IEC 62600-30 guidelines for measuring harmonic distortion were applied to sea trial testing from the MWPP and laboratory testing at the Lir NOTF. The laboratory testing was designed to mimic conditions at the MWPP, as both systems have LV connections to the grid and similar resource conditions. The resource classifications for the trial presented here were based on H_s . Low energy seas are $H_s < 1.25$ m; medium energy seas are $1.25 \text{ m} \leq H_s < 2.5$ m; high energy seas are $H_s \geq 2.5$ m. The IEC 62600-30 recommends that at least five datasets under each resource

classification are analysed. For the sea trials, 24 datasets, collected over a period of four months from January through April 2013, were analysed, with eight datasets for each resource. For the laboratory trials, 14 datasets were generated of the most common sea states observed annually. The datasets were collected and processed according to the IEC documentations.

2.1. IEC 62600-30 Harmonic Current Analysis Methods

IEC 62600-30 documentation stipulates that the emission of current harmonics needs be measured and recorded. As recommended in IEC 62600-30, the harmonic distortion analysis was based on IEC 61000-4-7: testing and measurement techniques—general guide on harmonics and interharmonics measurements and instrumentation for power supply systems. The harmonic distortion analysis had three separate determinations: harmonic distortion, interharmonic distortion, and high-frequency harmonic distortion. The analysis and observations were based on the fast Fourier transform (FFT) of the original current signal, as outlined in the IEC 61000-4-7 documentation, this includes setting the duration of the time window for the FFT at 200 ms. The FFT of the original signals was performed using the 'fft(x)' function developed by The Mathworks, Inc. for their MATLAB software.

The harmonic distortion refers to signals at frequencies which are an integer multiple of the fundamental frequency of the power system. The power systems evaluated in this report had a fundamental frequency of 50 Hz, so the harmonics of the system were 100 Hz, 150 Hz, 200 Hz, up to and including 2.5 kHz. Interharmonics refers to spectral components with frequencies between two consecutive harmonic frequencies. High-frequency harmonics refers to those signals with frequencies above 2 kHz and below 50% of the sampling frequency. The datasets were generated over a period of 10 minutes. The sampling frequency was 15 kHz for the sea trial datasets, and the sampling frequency was 20 kHz for the laboratory datasets.

2.1.1. Determination of Harmonic Currents Below 2.5 kHz

Harmonic distortion below 2.5 kHz represents the harmonic orders from $h = 2$ to $h = 50$ for a 50 Hz signal, where h is the integer ratio of a harmonic frequency to the fundamental frequency of the power system.

For the assessment of harmonics, the output of the FFT was grouped with the sum of the squared intermediate components between two adjacent harmonics, as shown in Equation (1). The FFT analysis assumed a stationary signal, but the magnitude of power systems tends to fluctuate, spreading out the energy of the harmonic components to adjacent spectral component frequencies [15]. To account for the fluctuations in signal, the output components for each 5 Hz of the FFT were grouped using Equation (1), as given in IEC 61000-4-7. The resulting harmonic subgroup of order h has a magnitude:

$$I_{sg,h}^2 = \sum_{k=-1}^1 I_{C,(N \times h) + k}^2 \quad (1)$$

where $I_{sg,h}$ is the resulting Root Mean-Square (RMS) current value of the harmonic subgroup, h is the integer multiple of the fundamental frequency that represents the harmonic order, $I_{C,(N \times h) + k}^2$ is the RMS value of the spectral component corresponding to an output bin of the FFT, N is the number of power supply periods within the window, h is the harmonic group frequency order, and k is the order of the spectral components. The output components for each 5 Hz of the FFT were grouped by Equation (1) as shown in Figure 1 to improve the assessment accuracy of the current, as directed by IEC 61000-4-7 [15].

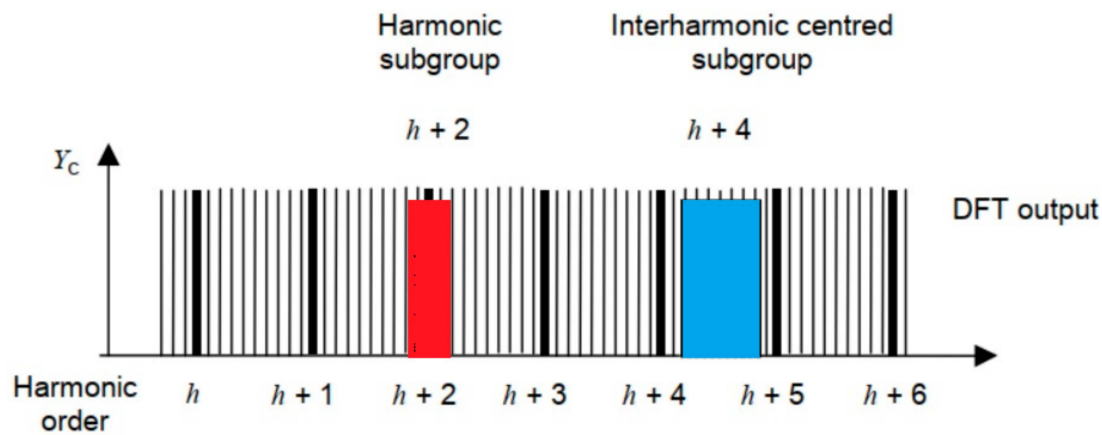


Figure 1. Illustration of the harmonic subgroups in red and interharmonic centred subgroups in blue [15].

The resulting RMSs of the amplitude of the current harmonic subgroups were used to determine the harmonic current distortion for each harmonic from $h = 2$ to $h = 50$. IEC 62600-30 states that harmonic currents below 0.1% of the device rated current, I_r , for any of the harmonic orders need not be reported. Equation (2) was used to determine the normalised currents of a given harmonic order and if those currents need to be reported:

$$\left(\frac{I_{sg,h}}{I_r}\right)\% = \frac{\sqrt{\sum_{k=-1}^1 I_{C,(N \times h) + k}^2}}{I_r \sqrt{2}} * 100, \quad (2)$$

where I_r is the rated current of the wave energy converter. Again, the output components for each 5 Hz of the FFT were grouped by Equation (1), as shown in Figure 1.

2.1.2. Determination of Interharmonic Currents Below 2.5 kHz

Interharmonics below 2.5 kHz represent the RMS values of current components whose frequencies are not an integer of the fundamental, which appear as discrete frequencies of a wide-band spectrum [16]. A grouping of the spectral components in the interval between two consecutive harmonic components forms an interharmonic group [15].

Interharmonic components are caused primarily by two sources: variations in the amplitude and/or phase angle of the fundamental component and/or of the harmonic components, and power electronics circuits with switching frequencies not synchronised to the power supply frequency and power factors correctors. Potential effects include additional torques on motors and generators, disturbed zero crossing detectors, and additional noise in inductive coils.

Spectral components associated with interharmonics usually vary in both magnitude and frequency. Grouping them provides an overall value for the spectral components between two discrete harmonics, which includes the effects of fluctuations of the interharmonic components. To further reduce the effects of amplitude and phase angle fluctuations, components immediately adjacent to the harmonic frequencies that the interharmonics were between were excluded by using Equation (3), which is given in Annex A of 61000-4-7:

$$I_{isg,h}^2 = \sum_{k=2}^{N-2} I_{C,(N \times h) + k}^2 \quad (3)$$

where $I_{C,(N \times h) + k}^2$ is the RMS value of the spectral component corresponding to an output bin of the FFT that exceeds the frequency of the harmonic order h , $I_{isg,h}^2$ is the RMS value of the interharmonic current centred subgroup of order h .

The resulting RMSs of the amplitude of the current interharmonic subgroups were used to determine the interharmonic current distortion between harmonics from $h = 2$ to $h = 40$. Equation (4) was used to determine if the normalised currents of a given harmonic order need to be reported:

$$\left(\frac{I_{isg,h}}{I_r}\right)\% = \frac{\sqrt{\sum_{k=2}^{N-2} I_{C,(N \times h)+k}^2}}{I_r \sqrt{2}} * 100, \quad (4)$$

2.1.3. Determination of High-Frequency Harmonic Currents

High-frequency harmonics are components in signals with frequencies above the 40th harmonic, which is 2 kHz for a 50 Hz system. They can be caused by several phenomena, including Pulse-Width Modulation (PWM) control of power supplies at the mains side connection, emissions like mains signalling, feed-through from the load or generator side of the power converters to the mains system side, and oscillations due to commutation notches. The measurement of these components is grouped into predefined frequency bands based on the signal energy of each band.

The FFT output was grouped into 200 Hz bands, beginning at the first centre band above the harmonics range. For the analysis of 50 Hz signals, the first centre band frequency was 2100 Hz. The RMSs of the amplitude of the high-frequency current bands were used to determine the harmonic current distortion between harmonics from $f = 2100$ Hz to $f = 7500$ Hz for the sea trials and $f = 2100$ Hz to $f = 8900$ Hz for the laboratory trials. Equation (5) was used to determine if the normalised currents of a given harmonic order need to be reported:

$$\left(\frac{I_{hff,f}}{I_r}\right)\% = \frac{\sqrt{\sum_{k=b-95}^{b+100} I_{C,f}^2}}{I_r \sqrt{2}} * 100, \quad (5)$$

where $I_{hff,f}$ is the current amplitude at the frequency of f , I_r is the rated current of the marine energy converter, and $I_{C,f}$ is the RMS value of the current component C .

2.2. Mutriku Wave Power Plant and SCADA System

The MWPP is composed of 16 fixed-type OWCs in an array. Each of the 16 OWC chambers has a two-stage Wells turbine and an 18.5 kW electrical generator that acts as the power take-off (PTO) system. The power generated by the wave energy plant is supplied to the local grid and accounts for approximately 400 MWh of carbon-free electricity annually [5].

Each OWC generator is controlled by an individual variable frequency drive (VFD), which allows the turbines to operate efficiently over a wide range of sea state conditions. The VFDs feed into a DC-bus, which is one of two within the plant. A single DC-bus accounts for eight generators, and each DC-bus supplies the grid through a 115 kW DC-AC converter that uses a VFD to sync to the AC output frequency with the local grid. The voltage and current outputs of a single DC-AC converter were monitored for the application of the IEC 62600-30 standards.

The SCADA system used to apply the IEC 62600-30 standards to the MWPP was connected to one of the 115 kW converters used to supply the grid. Measurements were taken from between the DC-AC converter and the radio frequency interference (RFI) filter that separated the grid from the converter. Voltage and current transducers installed within the plant's electrical system transformed the voltages and currents into signals that voltages that could be monitored by the SCADA system.

The main processing unit of the SCADA was a National Instruments (NI) cRIO-9082 operating NI Labview software. The cRIO-9082 is an eight-slot cRIO with a 1.33 GHz dual-core CPU, 2 GB of DRAM, 32 GB of ROM, and a Xilinx Spartan-6 LX150 FPGA. The cRIO was populated with NI-9239 analogue input modules with a voltage measuring range of -10 to 10 Volts. The NI-9239 has a sampling rate up to 50 kHz.

These specifications were vital for applying the IEC 62600-30 standards. To perform the harmonic analysis presented in this report, the IEC 62600-30 required a 10-minute continuous dataset sampled at 20 kHz. The Xilinx Spartan-6 LX150 FPGA along with the NI-9239 analogue import cards allowed for high-frequency sampling, but the sampling frequency was limited to 15 kHz, which is below the 20 kHz stipulated in IEC 62600-30. This limitation was due to the card being responsible for monitoring three signals. The number of signals handled by a single card affects the sampling rate, and for three signals, the maximum sampling rate was 16.67 kHz. The high-frequency harmonic analysis was limited to 7.5 kHz, rather than 10 kHz, because of the lower sampling frequency applied to the dataset. The sampling frequency and the 10-minute duration required required over 1 GB of memory per dataset. During deployment of the SCADA system, the 32 GB ROM had to be routinely cleared, with each dataset being moved to the cloud-based data storage system.

As the NI-9239 analogue input cards had a voltage range of ± 10 V, voltage and current transducers were installed as part of the SCADA system to convert the voltages and currents to signals that could be monitored by the analogue input cards. LEM supplied both the transducers for the voltage and current measurement to ensure continuity in the datasets. The voltage transducers were LEM DVL 750, which provide bipolar and insulated measurement up to 1125 V. The output of the transducers was a milliamp current with a set mA/V ratio to represent the measured voltage. The current transducers were LEM LA 305-S, which are Hall-effect closed-loop transducers, with a maximum range of ± 500 A. The output of the transducers was a milliamp current with a set mA/A ratio to represent the measured current. To produce signals that could be perceived by the cRIO, high tolerance resistors were placed in series with the current outputs of the transducers, as specified by the LEM provided technical data sheets for both transducers. Figure 2 shows the voltages and current transducers installed at the Mutriku Wave Power Plant; at the time of the photos, the voltage signals had not yet been wired to the voltage transducers.

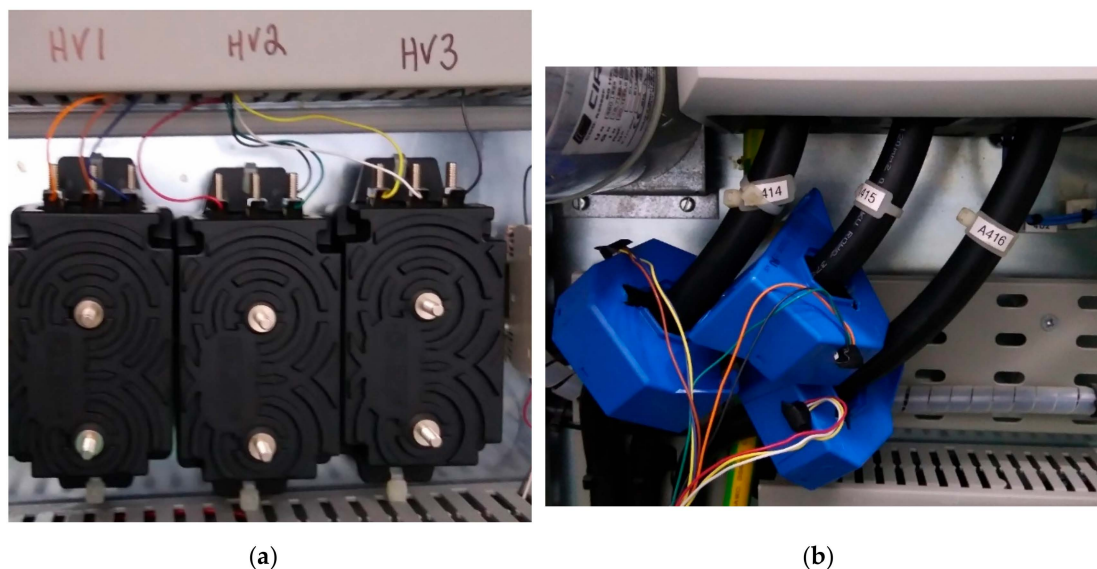


Figure 2. The voltage and current transducers installed in the Mutriku Wave Power Plant: (a) three LEM DVL 750 voltage transducers; (b) three LEM LA 305-S current transducers.

The voltage and current transducers were retrofitted into the already operational MWPP, and there were difficulties with the physical placement of the current transducers due to space and wiring requirements. Ideally, the voltage and current measurements for the application of IEC 62600-30 should be taken after the RFI filter that was used to remove the high-frequency signal generated by the VFD in renewable energy generation systems. Unfortunately, the space and wiring requirements forced the installation of the transducers between the RFI filter and the grid-side VFD, and this influenced the results of the testing. Figure 3 is a single-line diagram for an individual DC-bus of the plant,

which shows the ideal placement of the voltage and current transducers in green and the actual placement of the voltage and current transducers in red.

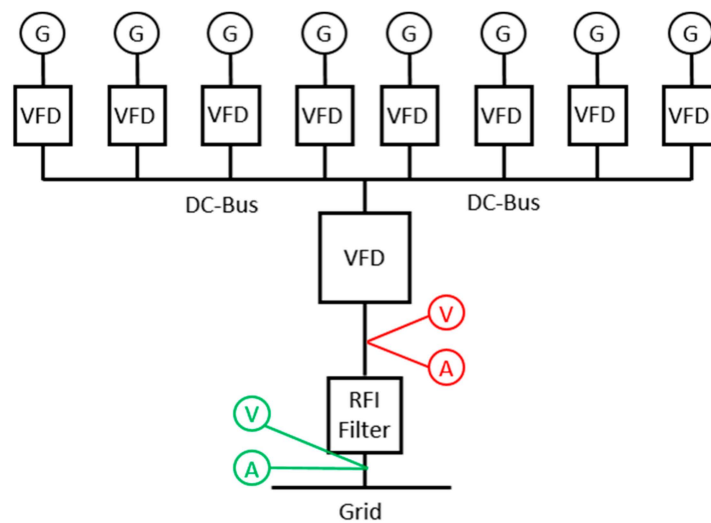


Figure 3. Mutriku wave power plant single line drawing showing how the eight generators were connected to the grid via a single DC-bus and the ideal and actual placement of the transducers.

2.3. Lir National Ocean Test Facility Electrical Lab and SCADA System

The electrical laboratory at the Lir NOTF at UCC includes a medium speed rotary emulator. The rotary emulator, shown in Figure 4, is an electromechanical system used to mimic the rotating electrical power take-off (PTO) system of a renewable energy device. The emulator is composed of two electrical machines directly coupled by a mechanical shaft, with a torque transducer between them. The mechanical drive shaft also includes a stainless-steel flywheel that is connected to the system by a five-position gear box. The flywheel allows the drive shaft to be composed of one of five different inertial masses, which can be implemented to replicate the inertia of any system being tested. The prime mover, which is used to emulate the forces applied by the turbine, is a four-pole squirrel-cage induction machine (SCIM) with a rated power of 22 kW, a rated speed of 1467 rpm, and a rated torque of 143 Nm. The generator is a slip ring four-pole induction machine with a rated power of 22 kW, a rated speed of 1472 rpm, and a rated torque of 143 Nm. As described in [13], the generator rotor can be set in multiple configurations depending on the system which is being emulated. For the OPERA project, the rotor is configured as an SCIM.

The emulator includes HIL technology, allowing it to operate in real-time in conjunction with complex software modelling running on the MATLAB® Simulink® platform. The conditions modelled in the Simulink® software are relayed to the emulator to drive its behaviour, and the conditions of the physical testing equipment are fed back into the Simulink® model to affect the model and complete the loop. For the MWPP, the data sent to the emulator by the Simulink® model were turbine torque and chamber pressure, while the feedback from the emulator to the model was turbine speed. The emulator–HIL integration was meticulously characterised and verified to ensure accuracy of the software–hardware link [14].

As part of the OPERA project, the MWPP was modelled using Simulink® [12]. This model was combined with the HIL system at the Lir NOTF to facilitate the laboratory testing. During operation of UCC's emulator and model, the turbine input torque determined in Simulink® is sent to the Programmable Logic Controller (PLC) as a reference torque to drive the motor that acts as the turbine for laboratory testing. The controller for the generator resides on the PLC and determines the generator braking torque to extract power from the turbine and export electrical power to the grid.

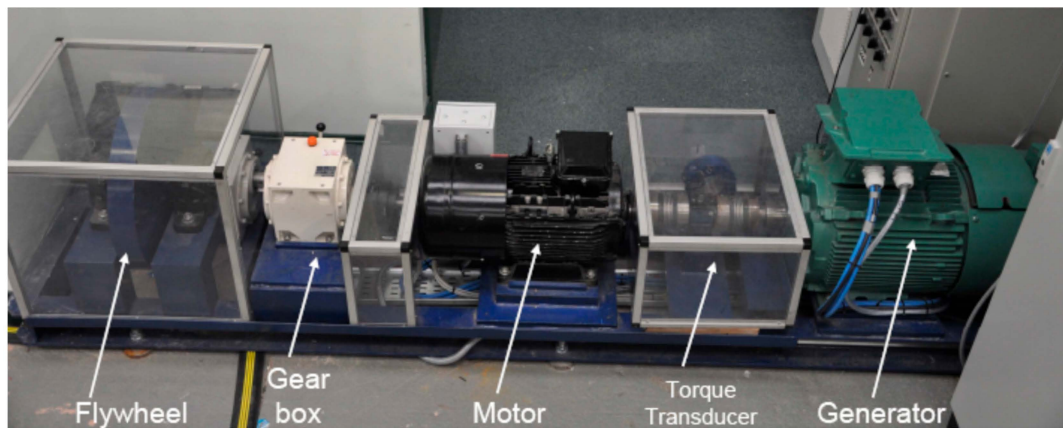


Figure 4. Drive train elements of the medium speed rotary emulator at the Lir NOTF laboratory.

The power rating of the turbine–generator PTO system installed at the MWPP was 30 kW, while the power rating of the turbine emulator and the generator of the HIL system was 22 kW. Due to this discrepancy, the model used for HIL testing had to be scaled down slightly to allow for testing. As is common in wave energy, the Froude scaling method was applied to the HIL model, with a scaling factor of 1:1.25.

The Lir NOTF electrical laboratory includes an integrated SCADA system that is very similar to the system installed at the MWPP, allowing for the laboratory generated datasets to be compared with the datasets from the sea trial testing. The Lir NOTF SCADA system also uses an NI cRIO-9082 running NI LabVIEW software for high-frequency data collection. The cRIO included NI-9225 cards rated for 300 V-RMS and NI-9239 cards with a voltage measuring range of -10 to 10 Volts. The NI-9225 cards were used to measure the line-to-neutral voltage at the point of common coupling (PCC) between the grid and the DC-AC converter output of the medium speed rotary emulator. The NI-9239 cards monitored the output of the current transducers for each of the three phases of the converter. The current transducers were LEM LA 55-P, with a current range of 0 to 50 A. The output of the current transducers was analogue current signals with a step-down ratio of $1000:1$. The cRIO was fit with high tolerance resistors rated to LEM specification to produce a voltage that could be monitored by the cRIO NI-9239 cards. The SCADA system in the lab allowed for the data to be collected at the recommended sampling frequency of 20 kHz for the 10 -minute window tests. The voltage and current transducers in the Lir NOTF were able to be installed after the RFI filter rather than before the filter. Figure 5 shows a single-line diagram of the laboratory arrangement, showing the placement of the current and voltage meters within the Lir NOTF electrical laboratory.

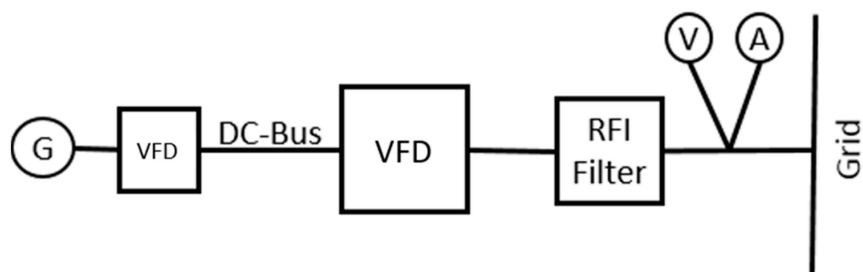


Figure 5. Single line drawing of the Lir NOTF emulator showing the placement of the voltage and current transducers.

3. Results of Harmonic Analysis for Sea Trial and Laboratory Generated Datasets

There were 24 datasets from the sea trials and 14 datasets from the laboratory testing that were analysed for current harmonic distortion. As the laboratory tests had to be modestly scaled and the power output of the grid side VFDs was different, the current data were normalised against rated

current for comparison. The datasets were spread across the three resource classifications, as identified in Section 2. Table 1 shows the significant wave height and energy period for both the sea trial and laboratory trial datasets, including the resource classifications. Although each dataset was processed and analysed individually, the results presented in this section represent the average values for each resource classification.

Table 1. Summary sea-state statistics for the datasets analyzed in the paper.

Sea Trials			Laboratory Trials			
Class	H_s (m)	T_e (s)	Class	H_s (m)	T_e (s)	
Low	0.50	17.80	Low	0.88	5.50	
	0.54	8.06		1.03	6.50	
	0.69	10.81		1.04	7.50	
	0.74	9.98		1.02	8.50	
	0.90	13.03		1.08	9.50	
	0.94	13.34		1.19	10.50	
	1.00	11.55		1.48	11.50	
Medium	1.09	10.12	Medium	1.81	12.50	
	1.33	12.53		2.07	13.50	
	1.39	16.43		2.11	12.50	
	1.58	15.51		2.59	14.50	
	1.86	13.61		High	2.88	15.50
	1.93	15.05			3.16	16.50
	2.11	12.89			3.20	11.50
High	2.23	14.33				
	2.41	13.85				
	2.62	14.31				
	2.64	13.65				
	2.66	13.28				
	2.74	15.54				
	3.22	16.19				
	3.35	15.65				
	3.69	15.68				
	4.14	16.81				

3.1. Measured Harmonic Currents Below 2.5 kHz

3.1.1. Sea Trial Datasets

As defined in Section 2.1.1., harmonic distortion below 2.5 kHz represents the harmonic orders from $h = 2$ to $h = 50$ for a 50 Hz signal, where h is the integer ratio of a harmonic frequency to the fundamental frequency of the power system. The harmonic current subgroups were identified via FFT. The RMS of the amplitude of the current harmonic subgroups was used to determine the harmonic current distortion for each harmonic from $h = 2$ to $h = 50$.

The harmonic current amplitude for the datasets generated during the sea trial was processed using the same FFT software referenced in Section 2.1. Table 2 shows the average harmonic currents as a percentage of the rated current of the converter, I_r , that reached the 0.1% of I_r reporting threshold for

the three resource classifications determined from the collected data based on Equation (2). Figure 6 shows a graphical representation of Table 1, including those harmonic currents below the 0.1% reporting threshold.

Table 2. Sea trial average reportable ratios of harmonic current amplitudes for each resource classification.

Average Harmonic Current Amplitude/Rated Current (I_h/I_r %)											
h	Sea State			h	Sea State			h	Sea State		
	Low	Medium	High		Low	Medium	High		Low	Medium	High
2	0.337%	0.374%	0.390%	13	0.336%	0.296%	0.273%	22	0.132%	0.138%	0.132%
3	2.713%	2.691%	2.819%	14	0.169%	0.161%	0.171%	23	0.111%	0.100%	0.098%
4	0.266%	0.281%	0.301%	15	0.469%	0.505%	0.601%	24	0.107%	0.112%	0.111%
5	1.581%	1.727%	2.044%	16	0.241%	0.240%	0.253%	33	0.120%	0.115%	0.120%
6	0.201%	0.202%	0.200%	17	0.338%	0.298%	0.312%	39	0.221%	0.238%	0.232%
7	0.401%	0.420%	0.457%	18	0.134%	0.132%	0.130%	41	0.218%	0.235%	0.228%
9	0.106%	0.097%	0.108%	19	0.223%	0.192%	0.193%	46	0.098%	0.093%	0.102%
11	0.305%	0.366%	0.339%	20	0.148%	0.152%	0.146%	50	0.277%	0.247%	0.267%

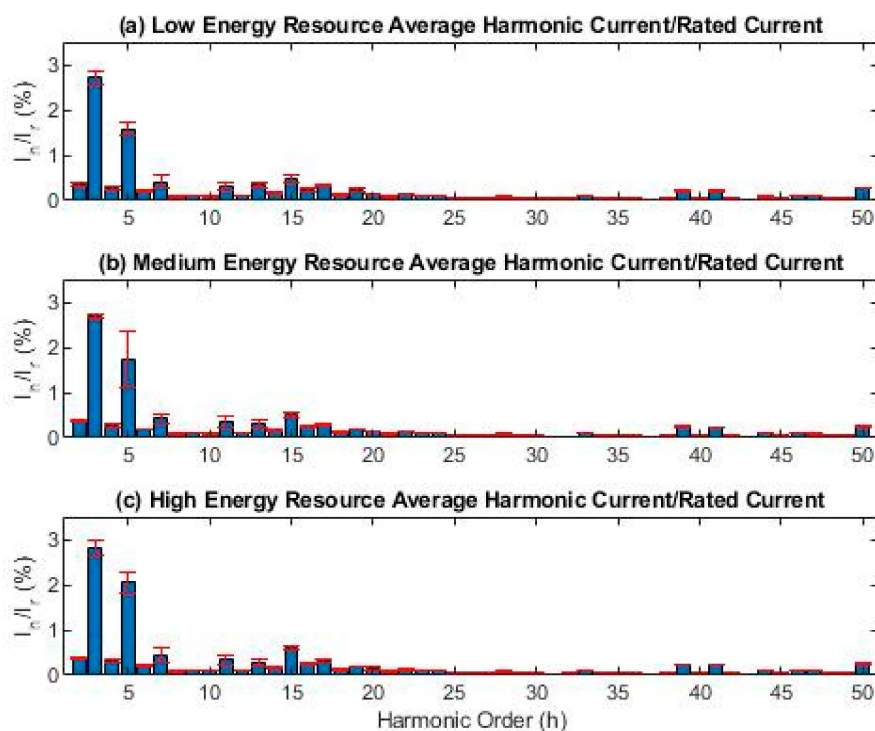


Figure 6. Sea trial average ratios of harmonic current amplitude to rated current for (a) low energy, (b) medium energy, and (c) high energy resource classifications, including error bars, which represent the standard deviation of the data averaged.

3.1.2. Laboratory Trial Datasets

The harmonic current amplitude for the datasets generated during laboratory testing was processed using the same FFT software that was applied to the sea trial data. Table 3 shows the average harmonic currents as a percentage of I_r , for the three resource classifications determined from the collected data, based on Equation (2). Figure 7 is a graphical representation of Table 3, including those harmonic currents below the 0.1% reporting threshold.

The most significant harmonic currents observed during the laboratory testing occurred at the fifth harmonic, 250 Hz, with additional notable harmonic currents occurring at the third harmonic, 250 Hz. The amplitudes of the remaining harmonic currents were below 1% of I_r with a number of them low enough that they need not be reported. For verification purposes, other notable peaks, those above 0.4% of I_r , in harmonic currents occurred at the 7th, 15th, 17th, 19th, 20th, and 26th harmonics. At harmonic orders above the 26th, only the 32nd, 37th, 38th, and 43rd harmonics reached the reporting threshold. As with the sea trial datasets, there was little variation in the observed harmonic currents across the three resource classifications, with small increases seen in the larger harmonic current amplitudes in the high energy classification. The amplitudes of the third and fifth harmonics exhibited any noticeable changes with changes in available energy in the sea condition, with the largest observed harmonic current for either trial occurring in the fifth order harmonic of the laboratory trial datasets.

Table 3. Sea trial average reportable ratios of harmonic current amplitudes for each resource classification.

Average Percentage Harmonic Current Amplitude/Rated Current (I_h/I_n %)											
h	Sea State			h	Sea State			h	Sea State		
	Low	Medium	High		Low	Medium	High		Low	Medium	High
2	0.322%	0.379%	0.421%	13	0.272%	0.315%	0.265%	22	0.066%	0.071%	0.071%
3	1.962%	2.138%	2.073%	14	0.491%	0.465%	0.480%	23	0.175%	0.262%	0.183%
4	0.336%	0.402%	0.452%	15	0.633%	0.633%	0.640%	24	0.048%	0.051%	0.053%
5	2.868%	2.658%	3.155%	16	0.129%	0.138%	0.150%	33	0.031%	0.032%	0.033%
6	0.203%	0.219%	0.249%	17	0.608%	0.485%	0.682%	39	0.032%	0.030%	0.032%
7	0.960%	0.766%	0.729%	18	0.151%	0.167%	0.189%	41	0.037%	0.037%	0.035%
9	0.365%	0.335%	0.310%	19	0.512%	0.594%	0.734%	46	0.029%	0.027%	0.027%
11	0.388%	0.462%	0.485%	20	0.547%	0.543%	0.537%	50	0.070%	0.074%	0.071%

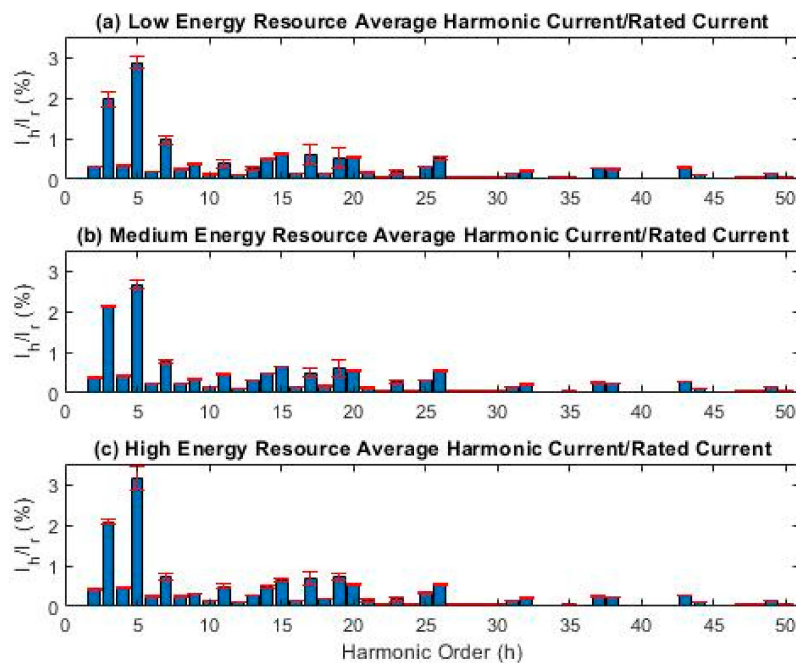


Figure 7. Laboratory trials average ratios of harmonic current amplitude to rated current for (a) low energy, (b) medium energy, and (c) high energy resource classifications, including error bars, which represent the standard deviation of the data averaged.

3.2. Determination of Interharmonic Currents Below 2.5 kHz

3.2.1. Sea trial Datasets

As defined in Section 2.1.2., interharmonics below 2.5 kHz represent the current RMS values of current components whose frequencies are not an integer of the fundamental, which appear as discrete frequencies of as a wide-band spectrum. A grouping of the spectral components in the interval between two consecutive harmonic components forms an interharmonic group, and the values of the interharmonic group current amplitude from the sea trials are presented in this section.

The groupings provide an overall value for the spectral components between two discrete harmonics, which includes the effects of fluctuations of the interharmonic components. To further reduce the effects of amplitude and phase angle fluctuations, components immediately adjacent to the harmonic frequencies that the interharmonics are between are excluded. The resulting RMS of the amplitude of the current interharmonic subgroups are used to determine the interharmonic current distortion between harmonics from $h = 2$ to $h = 40$. The interharmonic current amplitudes were determined with the same FFT software that was used to determine the harmonic currents.

Shows the average interharmonic currents as a percentage of I_r , for the three resource classifications determined from the collected data based on Equation (4). Figure 8 is a graphical representation of Table 4

Table 4. Sea trials average reportable ratios of harmonic current amplitudes for each resource classification.

Average Percentage Interharmonic Current Amplitude/Rated Current (I_{ih}/I_r %)											
ih	Sea State			ih	Sea State			ih	Sea State		
	Low	Medium	High		Low	Medium	High		Low	Medium	High
1	0.444%	0.684%	0.676%	14	0.173%	0.167%	0.173%	27	0.060%	0.063%	0.063%
2	0.325%	0.379%	0.377%	15	0.216%	0.220%	0.238%	28	0.048%	0.047%	0.048%
3	0.322%	0.346%	0.344%	16	0.128%	0.142%	0.148%	29	0.049%	0.050%	0.049%
4	0.240%	0.259%	0.264%	17	0.157%	0.118%	0.116%	30	0.037%	0.037%	0.039%
5	0.184%	0.194%	0.194%	18	0.102%	0.094%	0.095%	31	0.038%	0.037%	0.038%
6	0.136%	0.145%	0.150%	19	0.129%	0.129%	0.124%	32	0.060%	0.057%	0.054%
7	0.110%	0.116%	0.119%	20	0.076%	0.076%	0.076%	33	0.064%	0.063%	0.064%
8	0.083%	0.090%	0.093%	21	0.085%	0.085%	0.085%	34	0.037%	0.039%	0.038%
9	0.067%	0.075%	0.077%	22	0.074%	0.073%	0.073%	35	0.047%	0.052%	0.050%
10	0.059%	0.068%	0.067%	23	0.068%	0.066%	0.067%	36	0.038%	0.038%	0.038%
11	0.062%	0.068%	0.069%	24	0.053%	0.053%	0.052%	37	0.053%	0.054%	0.053%
12	0.078%	0.093%	0.082%	25	0.047%	0.047%	0.047%	38	0.101%	0.108%	0.097%
13	0.102%	0.100%	0.104%	26	0.043%	0.043%	0.044%	39	0.134%	0.153%	0.148%

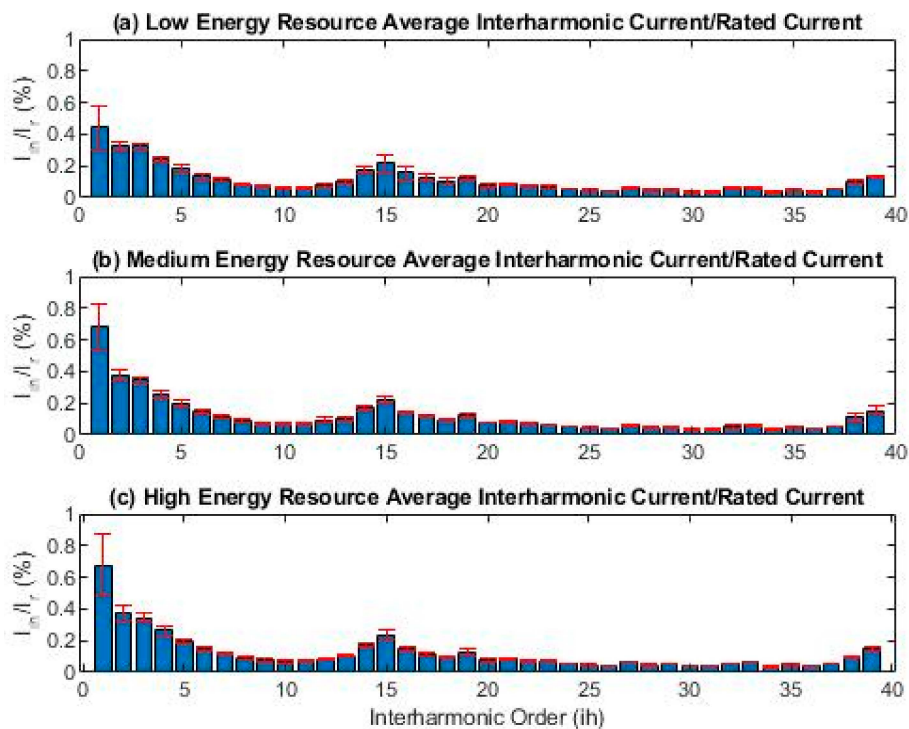


Figure 8. Sea trial average ratio of interharmonic current amplitude to rated current for (a) low energy, (b) medium energy, and (c) high energy resource classifications including errorbars that represent the standard deviation of the data averaged.

For the interharmonics, the most significant harmonic currents occur at the 1st interharmonic, which represents the window around 75 Hz. With the exception of the 1st interharmonic current, there is no discernible change in the interharmonic currents across the three resource classifications. There is a clear distribution across the interharmonic orders with peak currents at the 1st order, reaching a minimum in the lower interharmonics at the 10th order, reaching a secondary maximum at the 15th order, and sitting an overall minimum until the 39th order interharmonic where there is a final small peak in current. There is a 50% increase in the 1st order interharmonic currents observed from the low energy to the medium and high energy classifications, with little change in the observed interharmonic currents beyond the 1st order.

3.2.2. Laboratory Datasets

The interharmonic current amplitudes for the laboratory datasets were processed using the same software that was used for the sea trial datasets. Table 5 shows the average interharmonic currents as a percentage of I_r , for the three resource classifications determined from the collected data based on Equation (5). Figure 9 is a graphical representation of Table 5, which includes those currents that fall below the reporting threshold.

For the interharmonics, the most significant currents occur at the second and third interharmonic, which represents the window around 125 Hz and 175 Hz respectively. Including the below the 20th interharmonic order, there is an increase in the current amplitude of each interharmonic order with increasing energy available in the sea conditions. The increases are very small, with only the current amplitudes of the interharmonic orders first through fourth seeing increases above 0.1% of I_{ih}/I_r between the low energy and high energy conditions. Above the 20th order, there is little change between the sea state energy classifications. The interharmonic currents observed in the laboratory testing datasets were on average larger than those observed in the sea trial datasets. Like the sea trial interharmonics, there is little change in interharmonic currents over the resource classifications.

Table 5. Laboratory trials average reportable ratios of harmonic current amplitudes for each resource classification.

Average Percentage Interharmonic Current Amplitude/Rated Current (I_{ih}/I_n %)											
ih	Sea State			ih	Sea State			ih	Sea State		
	Low	Medium	High		Low	Medium	High		Low	Medium	High
1	0.432%	0.493%	0.519%	14	0.158%	0.169%	0.180%	27	0.048%	0.039%	0.041%
2	0.540%	0.567%	0.681%	15	0.154%	0.161%	0.183%	28	0.041%	0.035%	0.040%
3	0.543%	0.623%	0.668%	16	0.162%	0.178%	0.204%	29	0.036%	0.033%	0.035%
4	0.424%	0.500%	0.630%	17	0.170%	0.180%	0.231%	30	0.050%	0.044%	0.044%
5	0.343%	0.364%	0.405%	18	0.145%	0.162%	0.187%	31	0.064%	0.069%	0.069%
6	0.283%	0.302%	0.335%	19	0.123%	0.137%	0.153%	32	0.036%	0.042%	0.050%
7	0.245%	0.258%	0.284%	20	0.103%	0.113%	0.123%	33	0.033%	0.027%	0.030%
8	0.210%	0.220%	0.249%	21	0.071%	0.060%	0.057%	34	0.034%	0.030%	0.035%
9	0.184%	0.191%	0.210%	22	0.058%	0.063%	0.060%	35	0.029%	0.027%	0.030%
10	0.165%	0.173%	0.189%	23	0.047%	0.050%	0.051%	36	0.053%	0.050%	0.056%
11	0.149%	0.157%	0.175%	24	0.075%	0.068%	0.071%	37	0.076%	0.082%	0.088%
12	0.142%	0.148%	0.159%	25	0.133%	0.149%	0.152%	38	0.046%	0.045%	0.047%
13	0.175%	0.181%	0.193%	26	0.083%	0.093%	0.101%	39	0.030%	0.027%	0.028%

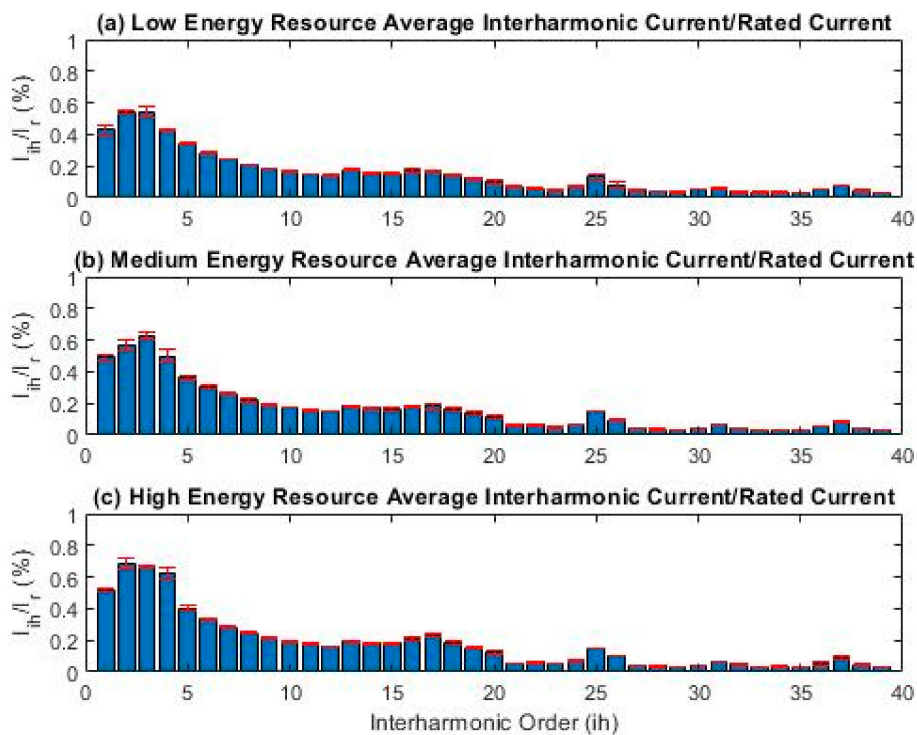


Figure 9. Laboratory trials average ratio of interharmonic current amplitude to rated current for (a) low energy, (b) medium energy, and (c) high energy resource classifications including errorbars that represent the standard deviation of the data averaged.

3.3. Determination of High-frequency Harmonic Currents

3.3.1. Sea trial Datasets

As defined in Section 2.1.3, high-frequency harmonic are components in signals with frequencies above the 40th harmonic, which is 2 kHz for a 50 Hz system. The measurement of high-frequency

harmonic components is grouped into predefined frequency bands based on the signal energy of each band according to IEC 61000-4-7.

The FFT output is grouped into 200 Hz bands beginning at the first centre band above the harmonics range. For the analysis of 50 Hz signals, the first centre band frequency is 2100 Hz. The RMS of the amplitude of the high-frequency current bands are used to determine the harmonic current distortion between harmonics from $f = 2100$ Hz to $f = 7500$ Hz for the sea trial datasets because the sampling frequency applied to the datasets was limited to 15 kHz, which would cause aliasing for frequencies above 7500 Hz.

The average high-frequency harmonic currents identified in the sea trial datasets for the three resource classifications are presented in Table 6 as a percentage of I_r , which is determined from the collected data based on Equation (5). Figure 10 is a graphical representation of Table 6.

The high-frequency signals prevalent in the data collected from the sea trials are directly related to the PWM switching of the grid side VFD used to create a 50 Hz sine wave to deliver power from the WEC to the grid, which has a switching frequency of 3 kHz. The largest currents are around the 3 kHz switching, with secondary currents at 6 kHz, which is the 2nd harmonic of 3 kHz. All other high-frequency harmonics currents are well under 1% of I_r . The current amplitudes observed at 2900 Hz and 3100 Hz represent the largest occurring harmonic current amplitudes for the sea trial datasets. This is largely influenced by the switching frequency of the VFD supplying power to the grid and the placement of the current transducers in relation to the RFI filter. There are no changes in the high-frequency harmonic currents across the three resource classifications.

Table 6. Sea trial average reportable ratios of high-frequency harmonic current amplitudes for each resource classification.

Average Percentage High-frequency Harmonic Current Amplitude/Rated Current (I_{high}/I_r %)											
f (Hz)	Sea State			f (Hz)	Sea State			f (Hz)	Sea State		
	Low	Medium	High		Low	Medium	High		Low	Medium	High
2100	0.316%	0.338%	0.331%	4100	0.273%	0.295%	0.283%	6100	0.794%	0.891%	0.828%
2300	0.211%	0.214%	0.222%	4300	0.205%	0.198%	0.204%	6300	0.672%	0.648%	0.657%
2500	0.443%	0.428%	0.446%	4500	0.137%	0.138%	0.135%	6500	0.072%	0.071%	0.074%
2700	2.195%	2.083%	2.225%	4700	0.098%	0.101%	0.098%	6700	0.111%	0.106%	0.108%
2900	4.062%	3.982%	4.095%	4900	0.176%	0.191%	0.178%	6900	0.218%	0.214%	0.222%
3100	4.003%	3.848%	3.959%	5100	0.186%	0.204%	0.193%	7100	0.189%	0.182%	0.187%
3300	1.745%	1.872%	1.982%	5300	0.099%	0.101%	0.099%	7300	0.106%	0.109%	0.115%
3500	0.377%	0.386%	0.398%	5500	0.161%	0.161%	0.161%	7500	0.084%	0.083%	0.085%
3700	0.249%	0.242%	0.251%	5700	0.748%	0.718%	0.734%				
3900	0.252%	0.272%	0.261%	5900	0.974%	1.071%	1.011%				

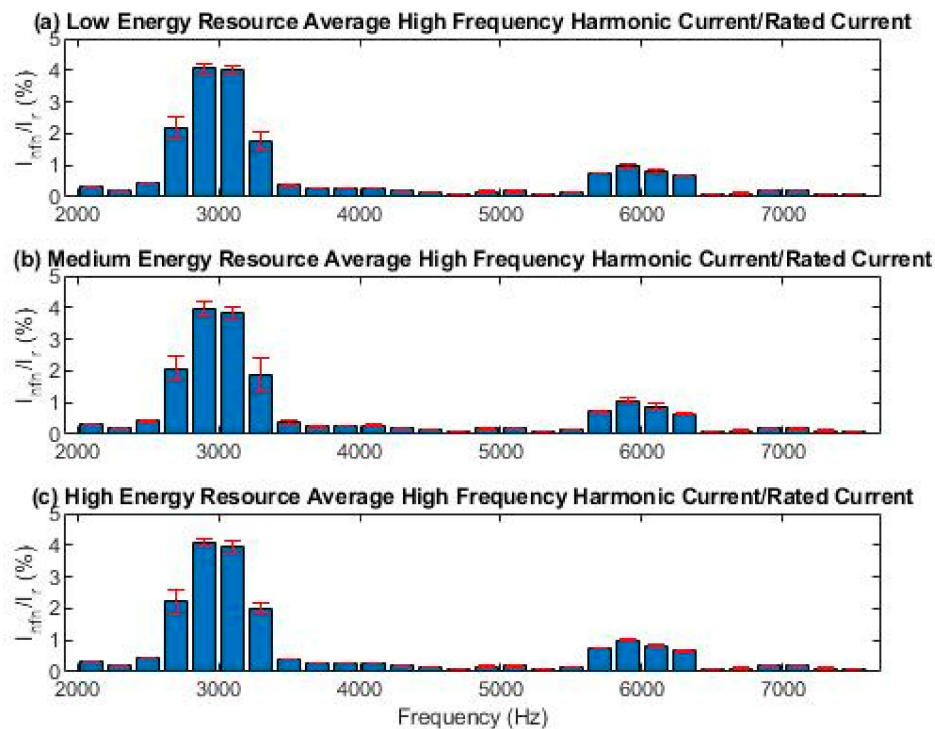


Figure 10. Sea trial average ratios of high-frequency harmonic current amplitude to rated current for (a) low energy, (b) medium energy, and (c) high energy resource classifications, including error bars, which represent the standard deviation of the data averaged.

3.3.2. Laboratory Datasets

The high-frequency current amplitudes for the laboratory datasets were processed using the same software that was used for the sea trial datasets. However, the laboratory datasets were sampled at 20 kHz, which is higher than the 15 kHz frequency used for the sea trial datasets. As a result, the RMSs of the amplitudes of the high-frequency current bands for harmonic current distortion could be determined up to $f = 9000$ Hz.

The average high-frequency harmonic currents identified in the laboratory trial datasets for the three resource classifications are presented in Table 7 as a percentage of I_r , which was determined from the collected data based on Equation (5). Figure 11 is a graphical representation of Table 7.

Like the high-frequency harmonic currents observed in the sea trial datasets, the high-frequency signals prevalent in the data collected in the dry laboratory datasets were directly related to the PWM switching of the grid side VFD used to create a 50 Hz sine wave to deliver power from the MEC to the grid, which had a switching frequency of 3 kHz. The effect of the RFI filter in the laboratory system is evident in these results, which show harmonic currents at the 3 kHz switching frequency to be four-times smaller than those observed in the sea trial datasets. The currents observed around 6 kHz were more similar to those seen in the sea trial datasets. Like the sea trials data, all other high-frequency harmonics currents in the dry laboratory testing were well below 1% of I_r .

Table 7. Laboratory trial average reportable ratios of high-frequency harmonic current amplitudes for each resource classification.

Average Percentage High-frequency Harmonic Current Amplitude/Rated Current (I_{hfh}/I_r %)											
f (Hz)	Sea State			f (Hz)	Sea State			f (Hz)	Sea State		
	Low	Medium	High		Low	Medium	High		Low	Medium	High
2100	0.325%	0.305%	0.313%	4500	0.225%	0.245%	0.237%	6900	0.103%	0.103%	0.106%
2300	0.114%	0.113%	0.114%	4700	0.140%	0.143%	0.140%	7100	0.144%	0.151%	0.146%
2500	0.191%	0.192%	0.189%	4900	0.350%	0.339%	0.318%	7300	0.092%	0.098%	0.099%
2700	0.279%	0.281%	0.271%	5100	0.256%	0.290%	0.282%	7500	0.157%	0.160%	0.156%
2900	1.075%	1.049%	1.013%	5300	0.170%	0.158%	0.160%	7700	0.091%	0.094%	0.092%
3100	0.746%	0.818%	0.802%	5500	0.529%	0.533%	0.533%	7900	0.142%	0.140%	0.142%
3300	0.281%	0.293%	0.283%	5700	0.147%	0.153%	0.160%	8100	0.146%	0.141%	0.143%
3500	0.304%	0.311%	0.310%	5900	1.654%	1.663%	1.654%	8300	0.068%	0.064%	0.060%
3700	0.124%	0.125%	0.123%	6100	1.305%	1.300%	1.280%	8500	0.095%	0.097%	0.096%
3900	0.381%	0.381%	0.377%	6300	0.143%	0.138%	0.137%	8700	0.200%	0.210%	0.210%
4100	0.413%	0.415%	0.413%	6500	0.354%	0.381%	0.368%	8900	0.304%	0.289%	0.267%
4300	0.155%	0.151%	0.144%	6700	0.198%	0.185%	0.184%				

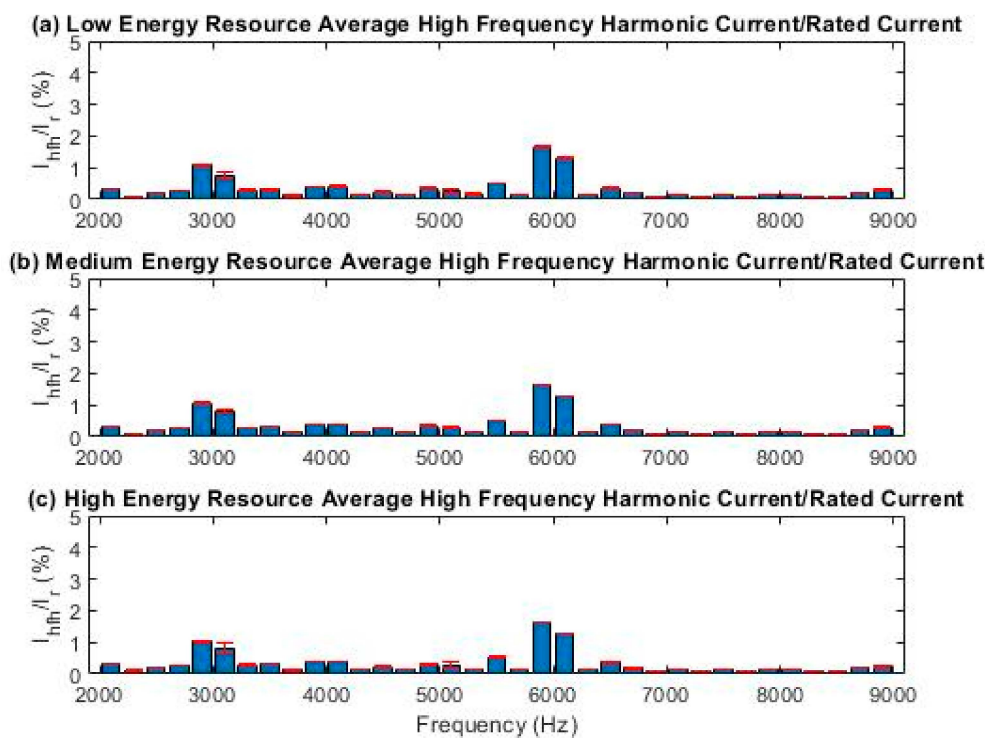


Figure 11. Laboratory trial average ratios of high-frequency harmonic current amplitude to rated current for (a) low energy, (b) medium energy, and (c) high energy resource classifications, including error bars, which represent the standard deviation of the data averaged.

4. Comparison of Sea trial and Laboratory Dataset Findings

To further investigate the validity of the results presented in Section 3, the harmonic, interharmonic, and high-frequency harmonic currents from the laboratory trials were compared against those determined from the sea trials performed at the MWPP. The data presented here represent the average of all the datasets for both the sea trial data and the laboratory generated data.

Figure 12 shows the harmonic, interharmonic, and high-frequency harmonic current amplitudes identified during testing and analysis, which includes data from sea-trials and laboratory trials side by side.

The most significant observations made from the data are that the general scale of the harmonic currents is very similar for both the sea trial and the laboratory generated data, with all harmonic currents falling below 5% of the rated current of the device. The observed harmonic currents were not always identical between sea trial and laboratory data, such as the third order harmonic being more prevalent in the sea trial data, while the fifth order was more prevalent in the laboratory data, but no two grid connections were identical.

The interharmonic currents fell below 1% of the rated current, with very similar results for both datasets. Again, the datasets were not identical, but the pattern of peaks at the lowest interharmonic orders, with a lull in currents around the tenth order before increasing again slightly around the 15th order, was apparent in both datasets.

The largest deviations in the two datasets could be seen at the high-frequency harmonics around 3 kHz. These deviations were directly related to the placement of the current and voltage transducers for the separate experiments. For the laboratory generated datasets, the current transducers were beyond the RFI filter, which was specifically designed to attenuate the 3 kHz switching frequency signal from the VFD, while the sea trial current transducers were located before the RFI filter, which led to the high harmonic current amplitudes observed around 3 kHz in the sea trial testing compared to the dry laboratory datasets. This indicates that the results from both tests are trustworthy and using HIL-based emulators can be used in early device development to evaluate potential harmonic distortion cause by MECs.

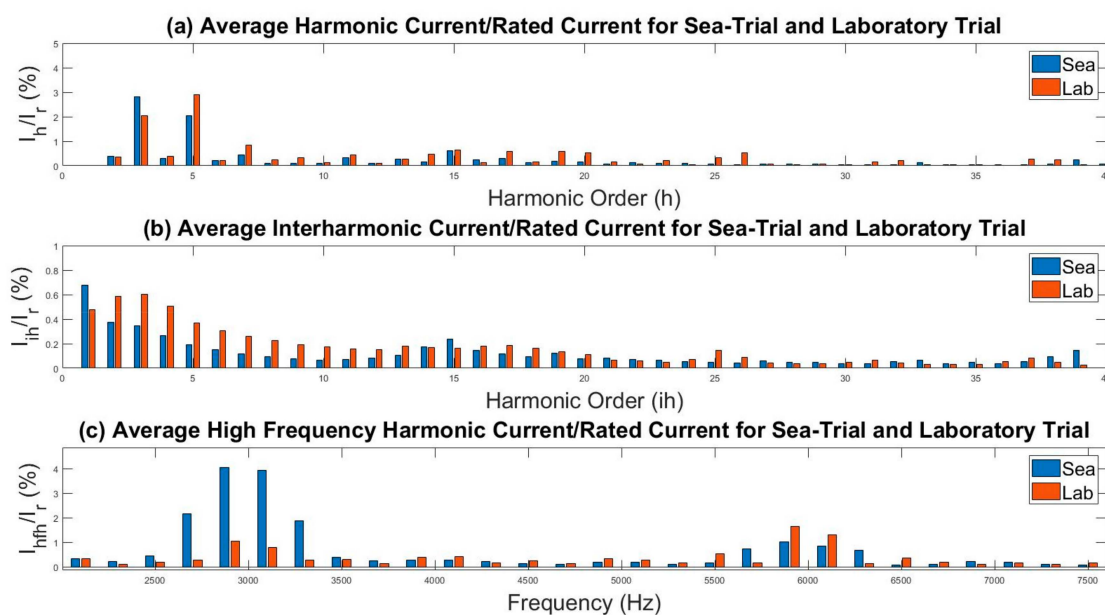


Figure 12. Average normalised harmonic currents observed during sea trial and laboratory trial testing.

Impact of RFI Filter on Data Measurements

The placement of the transducers in relation to the RFI filter for data collection at the MWPP affected the implementation of the IEC 62600-30 standards at the plant and the comparison of the plant datasets with the laboratory datasets. With the current and voltage transducers placed between the VFD and the RFI filter rather than on the grid side of the filter, the datasets were excessively influenced by the pulse-width modulation (PWM) switching of the VFD.

The RFI filters for use in renewable energy systems are specifically designed to attenuate high-frequency noise in signals caused by the PWM switching of VFDs use to generate 50 Hz AC

signals from a DC-bus. Figure 13 shows the current measurements taken from the MWPP SCADA system alongside the measurements from the emulator from the electrical laboratory at the Lir NOTF. The measurements from the Lir NOTF were taken from the output of an HIL WEC emulator, which is rated for 25 kW and features a back-to-back AC-DC/DC-AC converter similar to that installed at the MWPP. However, the laboratory generated data were measured by transducers installed on the grid side of the RFI filter rather than the VFD side of the filter. The SCADA system at the Lir NOTF uses the same NI and LEM equipment as was installed at the MWPP.

The difference between the two signals is mostly related to suppression of high-frequency noise by the RFI filter. The sea trial dataset had a more prevalent 3 kHz signal, but the 3 kHz signal could also be clearly observed in the dry laboratory generated dataset. This is reinforced by the results presented in Figure 12, where the largest discrepancies between the two datasets are the harmonic current amplitudes around the 3 kHz switching frequency.

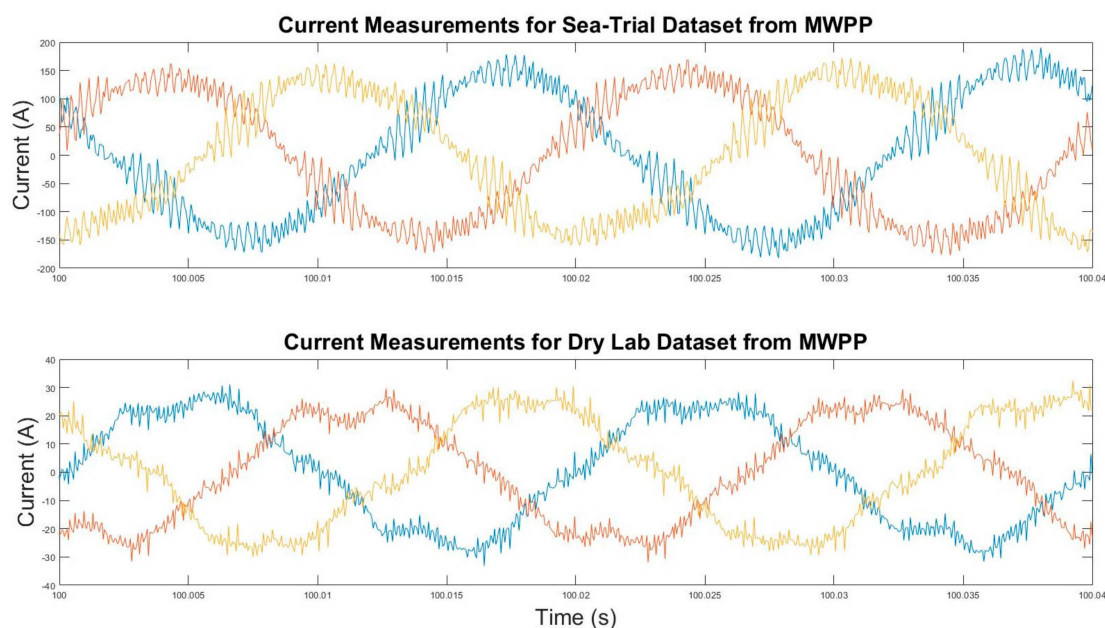


Figure 13. Current measurements from Mutriku Wave Power Plant (MWPP) sea-trials and Lir NOTF laboratory testing.

5. Conclusions

The research presented in this paper represents one of the first attempts to apply the IEC 62600-30 electrical power quality requirements for wave, tidal, and other water current energy converters standards to sea trials of a fully operational wave energy converter, while also using the data collected from the sea trials to attempt to evaluate the accuracy of using laboratory equipment to recreate real sea data. The harmonic distortion of the current created by an OWC was analysed across a range of sea conditions. The data were used to verify an OWC hardware-in-the-loop emulator, which was then used to expand the dataset. Successfully applying and meeting internationally accepted standards is an important step towards commercialisation for the wave energy industry. Several positive conclusions were drawn from the data analysed for this paper.

The IEC 62600-30 standards can be successfully applied to wave energy converters and can help provide confidence in the wave energy sector as it continues to move toward commercialisation.

- (a) Small scale oscillating water column wave energy converters can produce power that meets and exceeds internationally accepted standards for harmonic current distortion;
- (b) Sea state conditions represented by significant wave height and energy period have little effect on the harmonic currents produced by an oscillating water column wave energy converter.

As the overall energy available in the waves increases, the power injected into the grid increases. However, the corresponding increase in harmonic currents was modest;

- (c) While the differences between the sea trial and laboratory trial experimental setup limit the authority of the varication process, the early indication is that laboratory tests can accurately represent harmonic current distortion of sea trial testing. Further validation with more accurately replicated testing procedures needs to take place to confirm these initial results;
- (d) The values of the high-frequency harmonic currents around 3 kHz, which are caused by the PWM switching of the VFDs, highlight the importance of including an RFI filter in the development of the electrical power take-off for a wave energy converter.

Author Contributions: Conceptualization, Formal Analysis, Methodology, Validation, Visualization, J.K.; Data curation, E.A.; Project administration, Funding acquisition, P.R.M.; Investigation, Resources, Software, J.K. and E.A.; Supervision, J.K. and P.R.M.; writing – original draft preparation, J.K.; writing – review and editing, E.A. and P.R.M.

Funding: This research has received funding from the European Union’s Horizon 2020 research and innovation program under grant agreement No. 654444 (OPERA project).

Acknowledgments: The authors are grateful to the European commission for funding the OPERA projects as part of the Horizon 2020 framework. The authors also thankful to the Basque Energy Board (EVE) for providing technical information of Mutriku Wave Power Plant.

Conflicts of Interest: The authors declare no conflict of interest. The funders had no role in the design of the study; in the collection, analyses, or interpretation of data; in the writing of the manuscript, or in the decision to publish the results.

References

1. International Renewable Energy Agency (IRENA). *Renewable Energy Statistics 2018*; International Renewable Energy Agency (IRENA): Abu Dhabi, UAE, 2018.
2. Melikoglu, M. Current status and future of ocean energy sources: A global review. *Ocean Eng.* **2018**, *148*, 563–573. [[CrossRef](#)]
3. Uihlein, A.; Magagna, D. Wave and tidal current energy—A review of the current state of research beyond technology. *Renew. Sustain. Energy Rev.* **2016**, *58*, 1070–1081. [[CrossRef](#)]
4. Heath, T.V. A review of oscillating water columns. *Philos. Trans. R. Soc. A Math. Phys. Eng. Sci.* **2012**, *370*, 235–245. [[CrossRef](#)] [[PubMed](#)]
5. Torre-Enciso, Y.; Ortubia, I.; De Aguilera, L.L.; Marqués, J. Mutriku wave power plant: From the thinking out to the reality. In Proceedings of the 8th European Wave and Tidal Energy Conference, Uppsala, Sweden, 7–10 September 2009; Volume 710, pp. 319–329.
6. Falcao, A.F.; Henriques, J.C. Oscillating-water-column wave energy converters and air turbines: A review. *Renew. Energy* **2015**, *85*, 1391–1424. [[CrossRef](#)]
7. Liang, X. Emerging power quality challenges due to integration of renewable energy sources. *IEEE Trans. Ind. Appl.* **2016**, *53*, 855–866. [[CrossRef](#)]
8. Blavette, A.; O’Sullivan, D.L.; Alcorn, R.; Lewis, T.W.; Egan, M.G. Impact of a medium-size wave farm on grids of different strength levels. *IEEE Trans. Power Syst.* **2014**, *29*, 917–923. [[CrossRef](#)]
9. Blavette, A.; Kovaltchouk, T.; Rongère, F.; de Thieulloy, M.J.; Leahy, P.; Multon, B.; Ahmed, H.B. Influence of the wave dispersion phenomenon on the flicker generated by a wave farm. In Proceedings of the 12th European Wave and Tidal Energy Conference, Cork, Ireland, 27 August–1 September 2017.
10. Rajapakse, G.; Jayasinghe, S.; Fleming, A.; Negnevitsky, M. Grid integration and power smoothing of an oscillating water column wave energy converter. *Energies* **2018**, *11*, 1871. [[CrossRef](#)]
11. Henriques, J.C.C.; Sheng, W.; Falcão, A.F.O.; Gato, L.M.C. A comparison of biradial and wells air turbines on the Mutriku breakwater OWC wave power plant. In Proceedings of the ASME 36th International Conference on Ocean, Offshore and Arctic Engineering, Trondheim, Norway, 25–30 June 2017. [[CrossRef](#)]
12. Fajó, F.X.; Kelly, J.; Henriques, J.; Pujana, A.; Abusara, M.; Mueller, M.; Touzon, I.; Ruiz-Minguela, P. Numerical Simulation of Control Strategies at Mutriku Wave Power Plant. In Proceedings of the ASME 37th International Conference on Ocean, Offshore and Arctic Engineering, Madrid, Spain, 17–22 June 2018. [[CrossRef](#)]

13. Rea, J.; Kelly, J.; Alcorn, R.; O'Sullivan, D. Development and Operation of a Power Take Off Rig for Ocean Energy Research and Testing. In Proceedings of the 9th European Wave and Tidal Energy Conference, Southampton, UK, 5–9 September 2011.
14. Kelly, J.F.; Christie, R. Applying Hardware-in-the-Loop capabilities to an ocean renewable energy device emulator. In Proceedings of the IEEE 12th International Conference on Ecological Vehicles and Renewable Energies (EVER), Monte Carlo, Monaco, 11–13 April 2017; pp. 1–7. [[CrossRef](#)]
15. International Electrotechnical Commission. IEC Standard, Publication IEC 61000-4-7, Testing and Measurement Techniques-General Guide on Harmonics and Interharmonics Measurement and Instrumentation for Power Supply Systems and Equipment Connected Thereto. 2009. Available online: <https://webstore.iec.ch/publication/4228> (accessed on 20 September 2019).
16. International Electrotechnical Commission. IEC Standard, Publication 61000-2-1, Electromagnetic Environment for Low-Frequency Conducted Disturbances and Signalling in Public Power Supply Systems. 1990. Available online: <https://webstore.iec.ch/publication/4127> (accessed on 20 September 2019).



© 2019 by the authors. Licensee MDPI, Basel, Switzerland. This article is an open access article distributed under the terms and conditions of the Creative Commons Attribution (CC BY) license (<http://creativecommons.org/licenses/by/4.0/>).